MICROWAVE AND FAR INFRARED DIAGNOSTICS

A. Krämer-Flecken
Institut für Energie und Klimaforschung / Plasmaphysik, Forschungszentrum Jülich
D-52425, Jülich, Germany

I. INTRODUCTION

The measurement of plasma quantities is a difficult task since the plasma cannot be treated like *normal* material. The properties of a plasma with an electron density $\leq 1 \times 10^{20}\,\mathrm{m}^{-3}$ and temperatures up to several keV asks for sophisticated probes. Any measurement of plasma quantities with solid probes will yield interactions with the plasma and cause a perturbation of the measured quantity. Inside a hot plasma those methods are not applicable, since they cause a contamination which, on the long run, ends in a disruption of the plasma. Therefore it is necessary to use optical properties as refraction and reflection as tool for plasma diagnostic. Plasmas in fusion experiments are transparent when looked with human eyes. However, choosing the right wavelength where refraction effects are large, plasma properties can be accessed. The propagation of millimetre and sub millimetre waves in a plasma is quite sensitive to refraction and reflection. In addition those waves are less demanding regarding their installation requirements on fusion facilities either tokamak or stellerator due to the little space requirements. Microwave radiation can easily be guided in wave guides, either oversized or fundamental ones, which can be bend around corners and which widens the area of operation. Furthermore due to the rapid growing application in telecommunication, active as well as passive microwave components have become less expensive and more powerful.
Refraction and reflection allows to obtain information on the plasma density from the refractive index, when actively probed by microwaves. An other way of diagnosing a hot plasma is the measurement of the emitted radiation in the microwave range. With both methods main plasma parameters as the electron density and the electron temperature can be measured quite accurate and reliable. However, also the measurement of fluctuations in density and temperature and the determination of the plasma current density are possible with sophisticated microwave diagnostics. Using more than one observation location and performing cross correlation analysis yields information on the propagation of the plasma and the properties of turbulent structures can be achieved under certain assumptions. Those measurements contribute a lot on the understanding of turbulent transport and the interaction of different scales from microscopic (*turbulence*) to macroscopic (*flows*).
In the following section the propagation of electro magnetic waves in a plasma is reviewed. Sections III to VI are devoted to different diagnostic techniques. Section VII gives an outlook on future applications.

II. THE DISPERSION RELATION FOR THE PROPAGATION IN PLASMAS

Starting point is the *Appleton–Hartree* equation [1] which relates the refractive index N to the probing frequency ω.

$$\begin{aligned} N^2 &= 1 - \frac{A \cdot (1-A)}{1 - A - 1/2B^2 sin^2\theta \pm C} \\ A &= \frac{\omega_{pe}^2}{\omega^2} \quad ; \quad B = \frac{\omega_{ce}}{\omega} \\ C &= \left[\left(1/2B^2 sin^2\theta\right)^2 + (1-A)^2 B^2 cos^2\theta \right]^{1/2} \end{aligned} \tag{1}$$

Here ω_{pe} denotes the plasma frequency and ω_{ce} the cyclotron frequency:

$$\omega_{pe} = \sqrt{\frac{n_e e^2}{\epsilon_0 m_e}}; \quad \omega_{ce} = \frac{eB}{m_e \gamma} \tag{2}$$

γ takes into account relativistic effects, e denotes the electron charge, m_e the electron mass, n_e is the electron density and B the local magnetic field. The angle θ in Eq. 1 denotes the angle between the wave vector and the magnetic field.In the case $\theta = 0$ the propagation is parallel to the magnetic field. For $\theta = \pi/2$ we have a perpendicular propagation. In this case two solutions for the refractive index are possible, depending on whether the electric field vector of the wave $\mathbf{E}$ is parallel to the magnetic field (*O–Mode*) or perpendicular (*X–Mode*). The refractive index for both cases is given in equ. 3.

$$\begin{aligned} O-Mode \qquad N^2 &= 1 - \frac{\omega_{pe}^2}{\omega^2} \\ X-Mode \qquad N^2 &= 1 - \frac{\omega_{pe}^2 \left(\omega^2 - \omega_{pe}^2\right)}{\omega^2 \left(\omega^2 - \omega_{pe}^2 - \omega_{ce}^2\right)} \end{aligned} \tag{3}$$

All microwave diagnostics studying the propagation of millimetre waves are based on these equations, regardless of being applied in fusion plasmas, weather broadcast, or climate research.

III. INTERFEROMETRY

A standard tool for measuring the electron density n_e within a plasma is an interferometer. In this case we have the refractive index for *X–Mode* which is investigated with the additional assumption that $\omega_{ce}/\omega \ll 1$, neglecting the effects of the magnetic field. The measurement of the electron density is done by comparing the phase change of two wave trains, one travelling through the plasma, and another travelling through vacuum or air and which is used as reference. The phase change for a given wave number k an frequency is then given by:

$$\Delta\Phi = \int (k_{plasma} - k_0) dl = \int (N-1)\,\frac{\omega}{c} dl \qquad (4)$$

The above equation can be rewritten with the use of the critical electron density n_c at the cut–off layer where $N = 0$. From Eq. 2 we achieve the critical density as

$$n_c = \frac{\epsilon_0 m_e \omega^2}{e^2} \qquad (5)$$

yielding for the phase change:

$$\begin{aligned} \Delta\Phi &= \frac{\omega}{c} \int \left(\sqrt{1 - \frac{n_e}{n_c}} - 1 \right) dl \\ &\approx \frac{\omega}{2cn_c} \cdot \int n_e dl \end{aligned} \qquad (6)$$

Here, it has been assumed that $n_e \ll n_c$, truncating the expansion of the square root expression after the first term. Such a phase change can be measured by an interferometer.
Several types of interferometers exist. Two arm interferometer like *Michelson Interferometer* or *Mach-Zehnder-Interferometer* (Fig. 1) and multiple beam interferometer as *Fabry–Perot–Interferometer*.

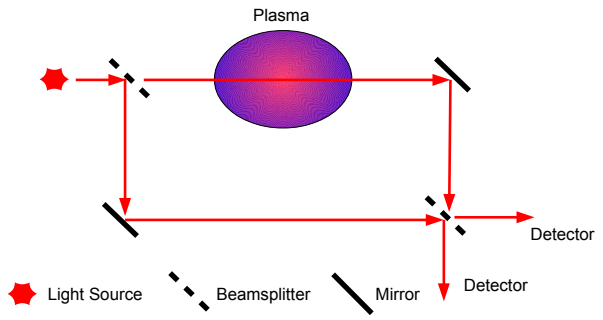

Figure 1: Schematic view of a Mach–Zehnder Interferometer

The major difference between the Michelson– and the Mach–Zehnder–Interferometer is the fact that the reference as well as the plasma path are only passed once in the Mach–Zehnder set–up. Two major drawbacks of all those types of interferometer are:

- The ambiguity of phase changes for $\Delta\Phi = n \cdot \pi$
- Amplitude variations due to refraction or absorption of the beam

To overcome those problems the frequency of the reference wave is shifted with a rotating grating. The detector will mix the two incoming frequencies from the plasma path ω_1 and the reference path ω_2 and yield an intermediate frequency $\Delta\omega_0 = \omega_1 - \omega_2$ and its higher harmonics. Such a detection scheme is called a heterodyne receiver. An additional phase change due to the plasma yield $\Delta\omega = \Delta\omega_0 + d\Phi/dt$. This allows a distinction between positive and negative phase changes.
To allow for interferometric measurements of n_e the following conditions have to be fulfilled.

- Sufficient power level for splitting the beam into radial separated chords and enough to detect at the same time 1 % modulation with a time resolution $\leq 100\,\mu s$
- No cutoffs or resonances in the plasma for the desired frequency deduced by the maximum n_e which can be achieved
- Small angular deviation of the beam ($\alpha \leq 10\,\text{mrad}$)

An interferometer–polarimeter of Mach-Zehnder type [3] using a HCN-laser operating at a frequency of 800 GHz was installed at TEXTOR (see Fig. 2) where the signals are detected by pyroelectric detectors. As can be seen from Eq. 6 the interferometric phase shift is integrated along the line of sight yielding line averaged densities. However, of importance is the local electron density and its profile. To fulfill an accurate calculation of the local density from the phase shift, tomographic methods have to be used. The phase shift has to be measured within a poloidal cross section of the tokamak with several chords at different radial position. Therefore assumption about the shape and symmetry of the plasma have to be made. With an inversion procedure (Abel–Inversion) a density profile is calculated.
A draw back of the previous mentioned short wavelength is the sensitivity to vibrations of the interferometer frame. Already small vibrations yield a disturbance of the path length and therefore an error in the phase measurement. To overcome this problems (i) the optics has to be mounted in a rigid frame or (ii) two different wavelength should be used. The shorter wavelength measures the disturbance of the diagnostic and the longer wavelength measures the refractive effects due to the plasma. In more sophisticated experiments it is even possible to detect the disturbance of the path length and try to adjust the path length by a moving mirror. Another problem is the bending of the chords. The plasma acts itself as a lens. Specially in the case of steep density gradients at the plasma boundary the changes in the refractive index will be quite large. As a consequence

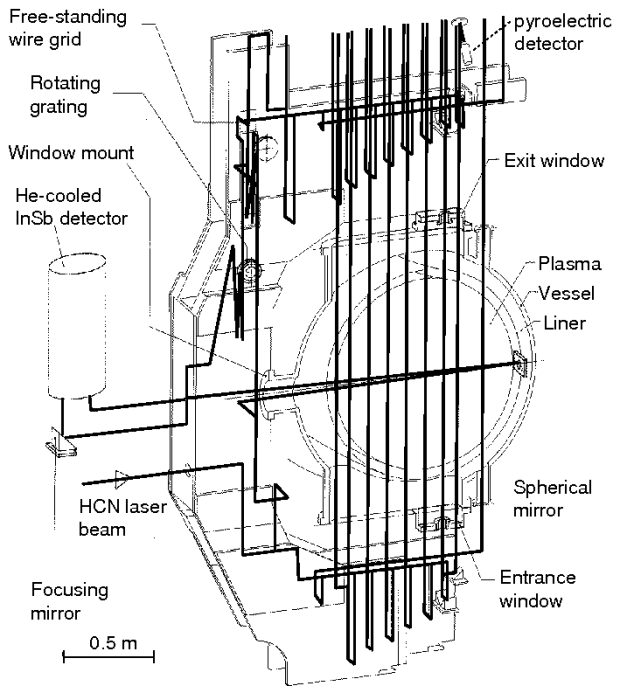

Figure 2: Schematic view of the nine channel HCN–interferometer–polarimeter as it was installed at TEXTOR. The thick lines show the optical path of the nine vertical, the horizontal and the reference channels.

the optical path length will increase and yield larger phase delays or the deviation will result in a loss of signal. In this case the inversion procedure will result in density profiles with higher edge densities and smaller one in the plasma center. From the geometrical point of view a multi chord interferometer is best suited for devices with circular plasma cross section. In D-shaped plasma only a few chords can be realized, mainly due to the restricted access from the top of the vessel. In this case other diagnostics are needed to calculate the required density profiles.

A. Dispersion Interferometry

The main draw back of a Mach–Zehnder or Fabry–Perot interferometer is the sensitivity to vibrations, specially for large devices like ITER and DEMO. This drawback can be overcome by using a second interferometer with a different wavelength and operated at the same path as the first one. or by using a dispersion interferometer [4, 5] which is not sensitive to phase changes due to vibrations. Probing and reference path use the same geometrical path but at different frequencies. The initial beam at frequency ω is partly doubled in frequency. Therefore frequency doubling crystals are used. Both waves at 1^{st} and 2^{nd} harmonic propagate through the plasma. After passing the plasma the 1^{st} harmonic is again doubled in frequency. In a next step the original frequency is filtered out. The interference pattern of the two waves at 2^{nd} harmonic are detected by a photo detector (see Fig. 3). The phase difference is the difference between twice the phase of the fundamental frequency and the phase of the 2^{nd} harmonic travelling through the plasma an can be expressed by:

$$\Delta\Phi = \frac{\omega}{c}\int \left[N(\omega) - N(2\omega)\right]dl \qquad (7)$$

With the equation for the refractive index N_O the phase change can be written as:

$$\Delta\Phi = \frac{3e^2}{8\pi\epsilon_0 m_e c^2}\lambda < n_e l > \qquad (8)$$

with λ being the probing wavelength and $< n_e l >$ the line integrated density. It should be noted that $\Delta\Phi$ increases with the used wave length. However, a large λ will be more limited by refraction. A compromise for the used wave length is found in CO_2-Laser at 28.3 THz corresponding to $\lambda \approx 10\,\mu$m. Such a system is installed e.g. at LHD [6] for density control. It has a temporal resolution of 300 µs and a sensitivity of $< n_e l >_{min} \leq 3 \times 10^{17}\,\mathrm{m}^{-2}$.

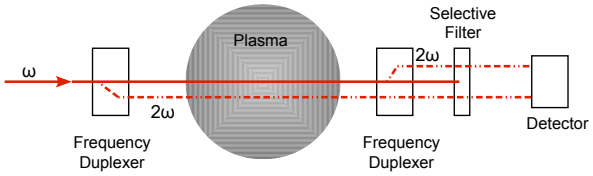

Figure 3: Principle scheme of a dispersion interferometer from [7].

IV. POLARIMETRY

Due to the magnetic field the refractive index is different for the two circular components of a linear polarized incident wave. In the case of a plasma current, generating a poloidal magnetic field, the interferometer–polarimeter set–up shown in Fig. 2 is sensitive to the parallel component of the poloidal magnetic field [3]. For a propagation of the wave parallel ($\theta = 0^o$) to the magnetic field component, the refractive index can be achieved from Eq. 1 retaining only first order terms in B, then we get:

$$N^2_{X,O} \approx 1 - A \pm AB cos\theta \qquad (9)$$

The difference in N causes a different propagation speed of the O- and X-mode wave, which causes a rotation of the electric field vector of a linearly polarized wave (*Faraday Rotation*). This is a rotation of the polarization plane. The phase change along the propagation direction (z–axis) is given by:

$$\Delta\Phi = \frac{\omega}{c}\left(N_X - N_O\right) z \qquad (10)$$

The Faraday rotation angle α depends only on Bdl and n_e. It can be expressed by the measured phase change and making use of Eq. 9 where only the first order terms in ω_{ce}/ω are considered.

$$\begin{aligned} \alpha &= \frac{\Delta\Phi}{2} = \frac{e}{2\, m_e\, c} \int \frac{n_e\, \mathbf{B}\cdot\mathbf{dl}}{n_e\,(1\ -\ n_e/n_c)^{1/2}} \\ &\approx \frac{e}{2\, m_e\, c} \int \frac{1}{n_c} \cdot n_e \mathbf{B}\cdot\mathbf{dl} \end{aligned} \quad (11)$$

This last approximation is valid if the ratio of electron density to critical density (n_c) is less than one. With the measurement of α the poloidal magnetic field can be estimated. The approximation is only depending on n_c which itself is a function of the used wavelength and the magnetic field, so that a numerical approach can be expressed by

$$\begin{aligned} \alpha\,[degree/cm] &= 1.5\times10^{-17}\ \lambda^2\,[mm] \\ &\times\ n_e\left[cm^{-3}\right]\ B\,[Gauss] \end{aligned} \quad (12)$$

After the measurement of the poloidal magnetic field at different radial positions the plasma current profile $j(r)$ as well as the q-profile can be estimated.

V. REFLECTOMETRY

Reflectometry measurements are based on the reflection of a probing microwave (ω_{ref}) at a cutoff layer (R_{co}) corresponding to a cut-off frequency (ω_{co}). The phase of the reflected wave contains information on the position of the cut-off layer and information on the density fluctuations [8]. At R_{co} the refractive index is $N = 0$ and depends on the polarization of the launched microwave (e.g. selected by the orientation of the launching and receiving antenna). The phase change can be calculated by Eq. 13,

$$\Phi = \frac{2\omega}{c} \int_{R_{edge}}^{R_{co}} N_{X,O}(R,\omega)dR - \frac{\pi}{2} \quad (13)$$

where c denotes the speed of light and $N_{X,O}$ the refractive index for X– or O–*mode* polarization as deduced from Eq. 3. At the R_{co} a phase jump of $\pi/2$ will arise. Reflectometry can be done in O–*Mode* and X–*Mode*, respectively. In case of X–*Mode* reflectometry N_X is a function of the magnetic field and it has the advantage that $n_e(r) = 0$ at $\omega_{co} = \omega_{ce}$ which offers a stable initialization condition for the measurement of density profiles. Another advantage of X–*Mode* reflectometry is the larger access in the radial range of the density profile. With O–*mode* reflectometry only half of the profile can be measured, since a reflectometer can not look behind the horizon. Concerning its accuracy the radial resolution depends on the density scale length and the fluctuation level. Reflectometry is therefore a good tool for plasma density profile measurements in the gradient region and for density fluctuation (turbulence) measurements. The detection of the reflected signal is similar to interferometry. The reflected and the reference signal at a slightly different are mixed. The resulting intermediate frequency serves together with the carrier as input for a quadrature detector which produces two output signals with 90° phase difference for each antenna. An overview on the diagnostic potential of the reflectometry can be found in [9].

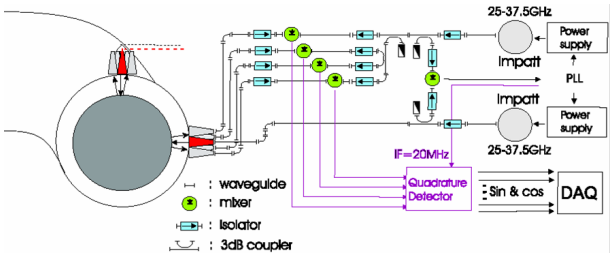

Figure 4: Schematic view and principal of the measurement of the heterodyne poloidal correlation reflectometer at TEXTOR. Microwave switches not shown in the figure allow to switch between signals from top and midplane array.

A. Density Profiles

The determination of the density profile was somewhat difficult in the past due to the large sweep times of the available microwave generators. The sweep time of the generators should be less or equal the life time of the fluctuation which is in the order of 10-20 µs. Today's technique allows a sweep time less than $10\mu s$ using hyperabrupt varactor tuned oscillators (HTO) [10, 11, 12]. In this case the fluctuations can be considered as frozen during one sweep of the oscillator. For profile measurements both polarizations can be used. Independent from the polarization the net time delay (τ) is given by:

$$\tau(f) = \frac{d\Phi}{d\omega} = f_B(\frac{df}{dt})^{-1} \quad (14)$$

Here f_B denotes the beat frequency of the reference and the reflected wave and $d\Phi/d\omega(f)$ denote the group delay. It is essential to know the frequency response on the evolution of the generator voltage, because it causes uncertainties in the estimation of the time delay. The density profile is reconstructed from an initialization procedure, which in case of O-mode could be quite complicated. Furthermore the sampling rate for such a system should be large, so that the fluctuations can be treated as frozen. In today set ups a sampling frequency up to 100 MHz and more is necessary to have a good frequency resolution during one sweep.

B. Turbulence and Rotation Measurements

In general reflectometry is most sensitive to long wavelength turbulence. With one launching and receiving antenna information on the phase fluctuation

can be retrieved from reflectometry. This can be related to density fluctuations as long as the phase fluctuation are small and not saturated. However, at the plasma edge the turbulence level becomes large and small angle scattering effects disturb the measurement. It makes the estimation of the turbulence level more complicated and sometimes even impossible.

The use of more than one receiving antenna surrounding the launcher allows the calculation of cross correlation as function of the toroidal and poloidal separation of antennae. The so called Correlation Reflectometry (CR) is often used to measure turbulence properties. This can be done either by using (i) an array of antennae measuring at toroidally and/or poloidally separated positions or (ii) by two reflectometers operating at different frequencies to obtain radial information on the turbulence structure and on the radial transport. A combination of both methods is possible as well. Using antennae arrays poloidally or toroidally separated, as shown in Fig. 4, yield further information on the poloidal or toroidal structure of the turbulence, e.g. poloidal correlation length ($\lambda_\perp$) and decorrelation time (τ_{dc}). However, the propagation time Δt between receiving antenna must fulfil the condition $\Delta t = \Delta s / v_\perp \leq \tau_{dc}$, where Δs is the distance between the correlated antennae. In Fig. 5 an example from poloidal CR shows the complex amplitude and cross phase spectra deduced from the quadrature detectors.

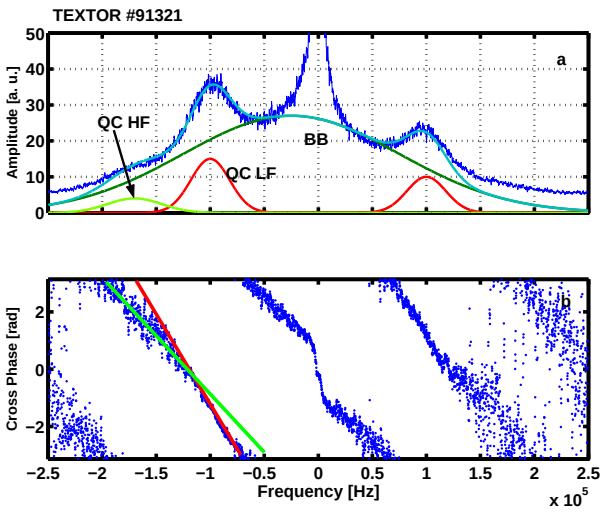

Figure 5: (**a**) Amplitude spectrum obtained from reflectometry showing the different fluctuation components. (**b**) The different propagation velocities are determined from the slopes in the cross phase spectrum.

From the complex amplitude spectrum different types of fluctuations can be recognized. Most pronounced are broad band fluctuations (BB)and the quasi coherent modes at low and high frequency (QC LF and QC HF). The different propagation velocities of the quasi coherent mode are obvious from the different slopes in the cross phase spectrum. For signals from poloidal separated antennae the angular velocity (Ω_{turb}) of the turbulence is measured from the crossphase (Φ) between the signals from two or more antennae [13].

$$\Omega = \frac{2\pi\ \alpha}{d\Phi/df}, \tag{15}$$

where α is the angle between the antennae. With the assumption that the additional phase velocity of the turbulence is small compared to the poloidal plasma velocity $\Omega_{turb} \approx \ \Omega_{Plasma}$ is valid. From the knowledge of the diamagnetic drift velocity (v_{dia}) the estimation of the radial electric field $E_r = (v_{turb} - v_{dia}) \cdot B$ where $v_{turb} = \Omega_{turb} \cdot r_c$, is possible. Here, r_c is the radius of the flux surface where the reflection takes place. Furthermore fluctuations in Ω_{turb} can be deduced if the sampling frequency is large enough compared to the frequency of the instability under investigation.

Recently it has been demonstrated that poloidally and toroidally separated antennae allow the determination of the inclination angle of the magnetic field line at r_c [14]. The projection of the distance of different antennae combinations on the direction of $v_\perp, B_\perp$ (see Fig. 6) yield different values for delay time Δt. With the assumption of a constant $v_\perp$ the ratio of the measured delay time is proportional to the magnetic pitch angle.

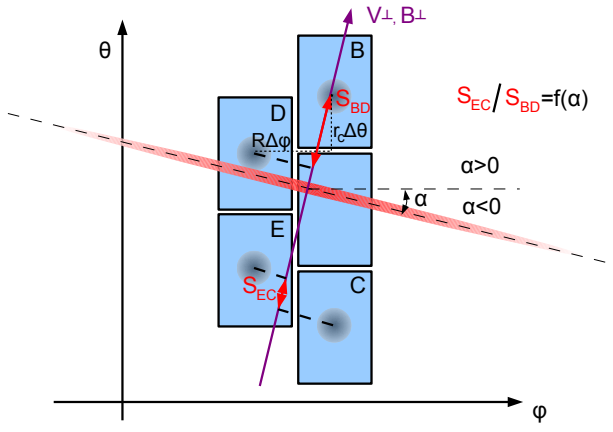

Figure 6: Schematic view of an antennae array. It shows the projection on the $v_\perp$ axis for combinations BD and EC.

An alternative method to deduce plasma velocity is the Doppler reflectometry [15]. Here the plasma velocity is deduced from the Doppler shift of the receiving microwave. Instead of measuring the 0^{th} order reflection which is used in standard reflectometry higher order diffraction is used for Doppler reflectometry (see Fig. 7). In most cases a tilted antenna is used for the launching and receiving microwave. In this case the tilting angle is adjusted to measure the -1^{st} order of diffraction and a monostatic antenna arrangement is sufficient. Such an set up is sensitive to

certain wave number values ($k_\perp$) depending on the tilt angle.

$$k_\perp = 2k_0 \sin \alpha_{tilt} \tag{16}$$

Here k_0 is the wave number of the probing microwave in vacuum. If the reflection layer in the plasma is propagating with a velocity $v_\perp$, a frequency shift of $\Delta\omega = -v_\perp \cdot k_\perp$ is observed. As for CR, Doppler reflectometry is able to deduce the radial electric field when the phase velocity of the turbulence can be neglected. Doppler reflectometry extents the measurement of turbulence properties to higher $k_\perp$ values and opens the window to electron temperature gradient driven turbulence. In case several Doppler reflectometry systems are operated at different frequencies cross correlation analysis can provide information on radial wavelength of the turbulence. A challenge

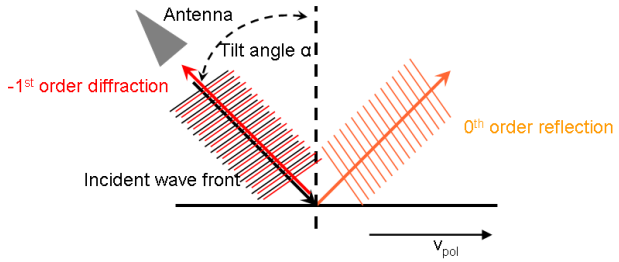

Figure 7: Principle of Doppler reflectometry. The 1^{st} order diffraction contains information on the propagation of the turbulence.

for Doppler reflectometry is the development of non-mechanical steerable antennae which can work at different centre frequencies and where a small variation of the centre frequency causes a wide variation in the tilt angle.
A further diagnostic mainly to study the small scale fluctuations is the upper hybrid resonance (UHR) scattering [16, 17]. The principle relies on the backscattering of a launched X-mode microwave at the UHR. After mixing the local and the time delayed received waves a spectrum is obtained. The amplitude of the spectral components depends on the time delay between the launched and the received wave and allows to estimate the wave number of density fluctuations. At the UHR also a conversion from X- to O-mode takes place. The backscattered O-mode component contains information on magnetic fluctuations. If the receiving X-mode antennae is replaced by a O-mode sensitive horn it is in principle possible to measure magnetic fluctuations as well.

VI. ECE DIAGNOSTIC

In this section the properties of the radiation emitted by the plasma are investigated. A review on the theoretical aspects of the propagation of microwave radiation in a plasma can be found in [18].

The radiation results from gyrating electrons at a frequency ω_{ce},

$$\omega_{ce} = \frac{e \cdot B}{m_e \cdot \gamma} \tag{17}$$

where γ is the relativistic mass factor. Due to relativistic effects the radiation is emitted also in higher harmonics of ω_{ce}. Having a spatial varying toroidal magnetic field as in a tokamak where $B_t \propto 1/R$ a relation between the emitted frequency and the location within the plasma is possible. In the case of a maxwellian energy distribution of the electrons the intensity of the emitted radiation can be related to the temperature. The emitted frequency spectrum can be described by Planck's equation. In a fusion plasma $\hbar\omega \ll kT_e$ is fulfilled and the Rayleigh–Jeans approximation can be used.

$$I(\omega) = B(\omega) = \frac{\omega^2 \cdot T_e}{8 \cdot \pi^3 \cdot c^2} \tag{18}$$

The measurement of the intensity of the emitted frequency alone is not sufficient. Also the transport of the radiation from its point of emission within the plasma to the observing antenna has to be taken into account. The transport of the radiation is described by

$$\frac{dI}{ds} = j(\omega) - I \cdot \alpha(\omega) \tag{19}$$

where s is the ray path and α the absorption coefficient and j the emissivity which are itself a functions of the frequency. The differential equation can be integrated yielding

$$I(s_2) = I(s_1) \cdot e^{-\tau_{21}} + \frac{j}{\alpha} \cdot [1 - e^{-\tau_{21}}], \quad \tau_{21} = \tau_2 - \tau_1 \tag{20}$$

where τ is the optical depth defined by:

$$\tau = \int \alpha(\omega) ds \tag{21}$$

The absorption coefficient is itself a function of local plasma parameters as n_e, T_e, the polarization of the wave (e.g. *X– or O–Mode*) and the harmonic number. With respects to cut-off's a suitable measurement of the electron temperature is performed for X-mode perpendicular propagation $\theta = 90^o$. In this case τ can be calculated from a WKB approach as outlined in paper by Bornatici [18].
For optical thick plasmas ($\tau \gg 1$) the first term on the right side of Eq. 20 becomes small, yielding:

$$T_e^{rad} = \frac{\omega^2 \cdot T_e}{8 \cdot \pi^3 \cdot c^2} \cdot \left(1 - e^{-\tau}\right) \tag{22}$$

As mentioned above, the propagation of electron cyclotron radiation in a plasma is limited by resonances and cut–off's. To find those positions we start from the *Appleton–Hartree relation* (Eq. 1) again. As already known from the first section the refractive index decides about cut–off and absorption frequencies for

the propagation in *X–Mode*. Cut–off and resonances are depending on the local B– and n_e–values. For $N^2 = 0$ a cut–off will reflect the wave. If $N^2 = \infty$ a resonance will absorb the wave. As can be seen from the Eq. 3 for *X-Mode* propagation perpendicular to the magnetic field we get the following equation for cut–off,

$$\omega_{CO1,2} = \sqrt{\frac{\left(2\omega_{pe}^2 + \omega_{ce}^2\right)}{2} \pm \sqrt{\frac{\left(2\omega_{pe}^2 + \omega_{ce}^2\right)^2}{4} - \omega_{pe}^4}} \tag{23}$$

and for resonances in the plasma we get:

$$\omega = \omega_{pe} \tag{24}$$

$$\omega = \sqrt{\omega_{pe}^2 + \omega_{ce}^2} \tag{25}$$

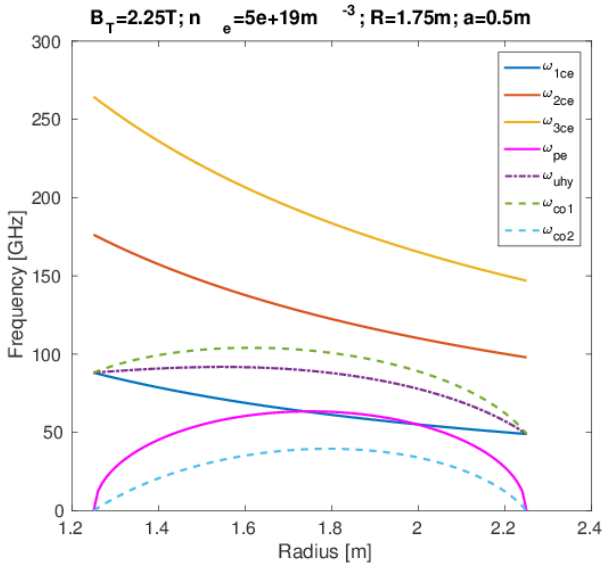

Figure 8: Cut–offs and resonances for a parabolic n_e–profile and $B_t = 2.25\,\mathrm{T}$ and $n_e^{max} = 5 \times 10^{19}\,\mathrm{m}^{-3}$ and $R_0 = 1.75\,\mathrm{m}$. Furthermore the first three harmonics of the electron cyclotron frequency are shown

From Fig. 8 it becomes clear that the 1^{st} harmonic can not be used for ECE-measurements since $\omega_{ce} \leq \omega_{pe}$ for $1.8 \leq R \leq 2\,\mathrm{m}$. But as long as the n_e is small enough the 2^{nd} harmonic is very well suited to measure the electron temperature. However for an increased density the cut–off frequency ω_{co1} overcomes the 2^{nd} harmonic. Already when the local n_e reaches $80 - 85\%$ of the cut–off density the 2^{nd} harmonic intensity drops, because of the divergence of the antenna beam [19]. In this case the 3^{rd} harmonic must be used. Disadvantage of this method is that the plasma is not optical thick for the 3^{rd} harmonic. Also multiple reflections of the radiation due to the plasma facing walls have to be taken into account. Therefore the first term in Eq. 20 is not zero and reflections from the wall have to be taken into account. The reflection coefficient ρ of the wall is material depending. For a wall covered by graphite tiles $\rho = 0.7$ is achieved [20]. The equation for the estimation of the temperature has to be modified

$$T_e^{rad} = \frac{\omega^2 \cdot T_e}{8 \cdot \pi^3 \cdot c^2} \cdot \frac{(1 - e^{-\tau})}{1 - \rho \cdot e^{-\tau}} \tag{26}$$

This method needs the knowledge of the local electron density and temperature when calculating the optical depth. The measurement of T_e from 3^{rd} harmonic is restricted to a small frequency range where the frequency range of 2^{nd} and 3^{rd} harmonic do not overlap (see Fig. 8). Otherwise a mixture of both harmonics will be measured and yield wrong T_e–values.
The radiation measurement at frequencies above $f = 70\,\mathrm{GHz}$ is difficult since the amplifier in this frequency range are noisy and the total amplification of the signal has to be around 80 dB, due to the low input power. To overcome this problem heterodyne radiometers are used for the measurement of T_e. They have a local oscillator for down conversion of the input frequency. As local oscillators Gunn-diodes made of GaAs are used because they are stable in frequency and have long lifetime compared with other microwave sources. The HF–frequency is mixed with the frequency of the local oscillator, yielding an intermediate frequency IF. The IF will pass a narrow filter with $\Delta f = 100 - 200 MHz$. This filter is responsible for the radial resolution of the radiometer. The noise temperature of such a radiometer is below $T_{sys} \leq 1000\,\mathrm{K}$. Unfortunately it is not possible to sweep the Gunn-diode over a large frequency range with constant output power therefore a broad-band mixer is used which covers the region from 2 GHz to 10 GHz. With a multiplexer and additional narrow bandpass filters T_e can be measured at several frequencies using only one LO-oscillator.This kind of radiometer has in general a higher noise temperature of $T_{sys} \approx 4000\,\mathrm{K}$. A typical example of a modern ECE diagnostic is shown in fig. 9. The system is installed at Tore Supra [21] and is operated with 4 local oscillators. The mixer cover a frequency range of 2 GHz to 18 GHz and after the mixer the signal is filtered and splits into 8 channels each. In total 32 radial positions can be measured with the system.
Beside heterodyne radiometer Michelson–Interferometer or a grated polychromator are used to measure T_e. The Michelson–Interferometer is mostly used to measure the emitted microwave radiation over a large frequency range (e.g. 1^{st} –4^{th} harmonic). This is done by a vibrational or pneumatically mirror in the device, allowing a scan over a large frequency range within $\approx 10\,\mathrm{ms}$. Since the power transferred to detector is very small the detector noise has to be reduced as much as possible by cooling with liquid helium.

VII. AN OUTLOOK TO FUTURE APPLICATIONS

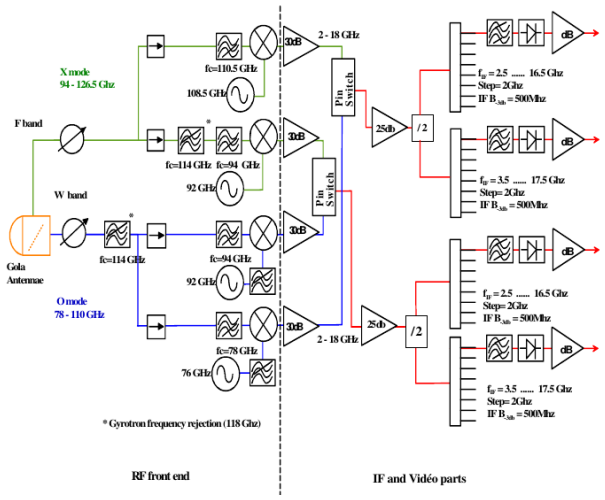

Figure 9: Modern set up of an ECE system at Tore Supra. The black dashed line shows thw separation between the high frequency and the IF part.

What are the main directions in the development of microwave diagnostics? The rapid increase in the development of microwave components for the automotive sector will make standard reflectometry diagnostics for today devices more cheap. Together with smaller antennae correlation measurements of turbulence structures could be realised easier. Furthermore the investigations towards 2-dimensional images from the plasma in the range of microwave frequencies needs advanced antennae technique. First experiments using ECE imaging are successful implemented at AUG [22]. Recent investigations of synthetic aperture microwave imaging for passive and active operation have been started at MAST [23]. The system operates with a time resolution of 10 µs and records images at 16 different frequencies. With such a system propagation as well as the pitch angle of turbulence can be studied

Beside the more technical oriented development new diagnostic ideas show up as the measurement of the local magnetic field from the pitch angle or equivalent to measure the ellipticity of the reflected beam cross-section (the axis is aligned with the magnetic field) using coherent detection techniques with two orthogonal components [24].

REFERENCES

1. I.H. HUTCHINSON, *Principles of Plasma Diagnostic*, (2nd ed.), New York, NY: Cambridge University Press, p. 109
2. N.C. LUHMANN, *Instrumentation and Techniques for Plasma Diagnostics*, in *Infrared and Millimeter Waves*, Vol. 2, Academic Press, New York, (1979)
3. H.R. KOSLOWSKI, H. SOLTWISCH, *Fusion Engeneering and Design*, **34-35**, 143-150, (1995)
4. F.A. HOPF et al, Opt. Lett., **5**, 386, (1980)
5. V.P. Drachev et al., Rev. Sci. Instrum. ,**64**, (1993), pp 1010–1013
6. Akiyama et al., 15th International Conference on Laser aided Plasma Diagnostic, October 13-19, 2011, Jeju, Korea, DOI:10.1088/1748-0221/7/01/C01055
7. P.A. BAGRYANSKY et al., Rev. Sci. Instrum. ,**77**, 053501, (2006)
8. R. Nazikian et al., Phys. Plasmas, **8**, (2001), pp 1840-1855
9. Special issue on reflectometry, Editor G.D. CONWAY, *Nucl. Fusion* **46**, (2006), No. 9
10. A. Silva et al., *Rev. Sci. Instrum.*, **67** ,(1996), pp 4138–4145
11. T. Tokuzawa et al., *Rev. Sci. Instrum.*, **68** ,(1997), pp 443–445
12. Ph. MOREAU, *Rev. Sci. Instrum.*, **71** ,(2000), pp 74–81
13. A. KRÄMER-FLECKEN et. al, *Nucl. Fusion*, **44**, (2004), pp 1143-1157
14. A. KRÄMER-FLECKEN et. al, *Rev. Sci. Instrum.*, **81**, (2010), 113502
15. M. HIRSCH et al., Rev. Sci. Instrum., **72**, (2001), pp 324–327
16. I. FIDONE et al., Phys. Fluids, **16**, (1973), 1680
17. D.G. BULYIGINSKIY et al., Phys. Plasmas, **8**, (2001), 2224
18. M. BORNATICI, *Plasma Physics*, **24**, No. 6, 629, (1982)
19. W.H.M. CLARK, *Plasma Physics*, **25**, No. 12, 1501, (1983)
20. A. KRÄMER–FLECKEN, P.C. DE VRIES, *Proceedings on the tenth workshop of ECE and ECRH*, p. 209, World Scientific, Singnapore, (1997)
21. J.L. Ségui et al., Rev. Sci. Instrum. **76**, 123501 (2005)
22. I.G.J. Classen et al., Rev. Sci. Instrum., **81**, 10D929 (2010)
23. V.F. Shevchenko et al., JINST, **7**, (2012), DOI: 10.1088/1748-0221/7/10/P10016
24. A. STEGMEIR et al., Fusion Engineering and Design **86** (2011) 29282942